JGR Earth Surface

RESEARCH ARTICLE
10.1029/2023JF007584

When Does the Concavity Index Constrain Stream Power Parameters?

Adam G. G. Smith[1,2] **and Matthew Fox**[2]

[1]School of Natural Sciences, Birkbeck, University of London, London, UK, [2]Department of Earth Sciences, University College London, University of London, London, UK

Key Points:

- The concavity index and *m/n* are not equivalent when there is spatial variation in relative rock uplift rate
- We present a new method to measure *m/n* that accounts for variation in rock uplift and erodibility
- By accounting for spatial variation, we are able to more accurately infer tectonic information from river networks

Supporting Information:

Supporting Information may be found in the online version of this article.

Correspondence to:

A. G. G. Smith,
adam.smith.20@ucl.ac.uk

Citation:

Smith, A. G. G., & Fox, M. (2024). When does the concavity index constrain stream power parameters? *Journal of Geophysical Research: Earth Surface*, *129*, e2023JF007584. https://doi.org/10.1029/2023JF007584

Received 5 DEC 2023
Accepted 26 AUG 2024

Author Contributions:

Conceptualization: Adam G. G. Smith, Matthew Fox
Data curation: Adam G. G. Smith
Formal analysis: Adam G. G. Smith
Investigation: Adam G. G. Smith
Methodology: Adam G. G. Smith
Supervision: Matthew Fox
Writing – original draft: Adam G. G. Smith
Writing – review & editing: Adam G. G. Smith, Matthew Fox

Abstract By defining the attributes of river networks, we can quantitatively extract records of climatic and tectonic changes from them. The stream power incision model (SPIM) provides a framework within which this can be achieved, as it facilitates the calculation of the relative rock uplift from river characteristics. One parameter that has been widely employed in tectonic and fluvial geomorphology is the channel steepness index, a metric that can represent the normalized rock uplift rate experienced by a river. However, to accurately infer the channel steepness index, we must accurately estimate *m/n*, the ratio between the two positive exponents of the SPIM. Present methodologies to constrain *m/n* rely on an assumption that rock uplift and erodibility are spatially invariant. These conditions are rarely present on Earth. In this study, we use a synthetic example and examples from the Siwalik Hills and Olympic Mountains to demonstrate how existing methodologies to constrain *m/n* produce systematic errors when there is spatial variation, and particularly spatial gradients, in the processes driving landscape evolution. To solve this problem, we present a methodology to estimate *m/n* based on a large river network inversion that accounts for spatial variation in landscapes. After demonstrating that the methodology can accurately recover *m/n* in our synthetic landscape, we show that our methodology can reconcile contrasting observations in the Siwaliks, and is critical to inferring accurate values of channel steepness index in the Olympic Mountains. This highlights the utility of large topographic inversions for investigating landscape dynamics.

Plain Language Summary Rivers move material across the Earth's surface in a process known as erosion. The amount of water in a river, and how quickly that water flows, controls how much a river can erode. To compare the number of erosion in different rivers, researchers created a stream power model. The stream power model allows researchers to measure features of rivers and put a number to the amount of erosion occurring in that river. Unfortunately, to do this we must know the values of some of the numbers in the model, which are known as *m* and *n*. However, this can be difficult to do if the amount of rainfall or rock uplift rate changes over the course of the river. In this paper, we solve this problem by introducing a new method to calculate *m/n*, which allows us to factor in changes in rock uplift and erodibility (a value that describes how easy it is for rivers to erode) along the river network. This allows us to recover the best fitting value of *m/n*.

1. Introduction

A principle of tectonic geomorphology is to take the shape of topography and infer the processes that created it. Rivers are particularly helpful in this endeavor, as they are found across much of Earth, are often the dominant drivers of topographic change in a landscape, and encode climatic and tectonic information within their morphology (Kirby & Whipple, 2012; Lague, 2014; Whittaker, 2012). Provided we can extract this information through parameterization and modeling of river processes, river networks represent a large data set that can be used to understand Earth surface processes.

River networks lend themselves to quantitative modeling as they follow a set of natural laws. River networks must flow downhill, and there is a relationship between upstream drainage area and slope that causes their slope to decrease as they do so (Hack, 1957; Morisawa, 1962). By defining the relationship between slope and area, we can compare the relative steepness of portions of rivers in the same network or different networks that have different upstream drainage areas. This is useful, as the relative steepness of a river can be a proxy for the relative rock uplift rate, which allows us to extract tectonic information from the Earth's surface (Kirby & Whipple, 2001, 2012; Smith et al., 2022; Wobus et al., 2006).

One popular way to extract the relative steepness of a river network is to use the stream power incision model (SPIM). This, however, requires constraining the ratio between the SPIM parameters m and n. Traditional methods to infer m/n require examining some length of a river network and assuming that tectonic, climatic, and geological variables that influence the form of river networks are constant over this length scale (Goren et al., 2014; Hergarten et al., 2016; Mudd, Clubb, Gailleton, & Hurst, 2018; Perron & Royden, 2013; Wobus et al., 2006). On Earth, this is rarely the case. Rock uplift rates deteriorate away from faults or fold axes, precipitation rates follow gradients due to orographic effects, and lithology varies on a variety of length scales (Burbank et al., 1996; Han et al., 2015; Reiners et al., 2003; Roe et al., 2002, 2003; Willett, 1999). As such, natural gradients almost always additionally contaminate estimates of the stream power parameters, beyond errors associated with noise and choice of methodology.

With the use of a synthetic, steady-state 2-D landscape and examples from the Siwalik Hills and Olympic Mountains, we demonstrate that existing methods to estimate m/n produce systematic errors when there is a spatial gradient in rock uplift or erodibility. We also present a new methodology to constrain the m/n based on a topographic inversion that can account for such spatial gradients. Using the same examples, we demonstrate that our method can accurately recover m/n, ensuring that subsequent measurements of geomorphic indices are also accurate. We demonstrate that our estimated m/n and channel steepness index values complement previous and independent observations of processes in our chosen natural landscapes, lending confidence to our results.

1.1. Flint's Law and the Stream Power Model

The relationship between the slope and upstream drainage area was described as a power law function by Hack (1957) and Morisawa (1962), before being formalized by Flint (1974). Flint's law, as it has become known, states that,

$$S = k_s A^{-\theta}. \tag{1}$$

where S is the slope, A is the upstream drainage area, θ is the concavity index, and k_s is the channel steepness index. This parameterization of river network data allowed researchers to describe differences in river networks in a quantitative manner.

The concavity index and channel steepness index can be extracted from slope and upstream drainage area data by performing slope-area analysis (Wobus et al., 2006). For a river at steady state, a regression fit through the log-transformed slope and area data yields two parameters: the concavity index and the channel steepness index. In this sense, the concavity index and channel steepness index are simply estimates made from topographic data to describe how quickly the gradient of a channel decreases downstream, and the relative steepness of the river, respectively.

The detachment limited stream power model (Howard, 1994; Howard & Kerby, 1983; Whipple & Tucker, 1999) can be recast into a version of Flint's law, allowing us to ascribe information about tectonics to the channel steepness index parameter. The stream power model states that the erosion rate,

$$E = KA^m S^n, \tag{2}$$

where A and S are the same as in Equation 1, m and n are positive exponents, and K is the erodibility, which combines many variables such as lithology, sediment size and climatic regime to describe the efficiency of fluvial incision. If a river network is in steady state and there is no change in the elevation of any location on a river network through time, the rock uplift rate and erosion rate must be balanced. We can therefore substitute E in Equation 2 for the rock uplift rate, u, and rearrange this equation to the power law described by Equation 1, where

$$S = \left(\frac{u}{K}\right)^{\frac{1}{n}} A^{-\frac{m}{n}}. \tag{3}$$

In the special case of spatially invariable values of rock uplift and erodibility, we can see that the channel steepness index is equivalent to $\left(\frac{u}{K}\right)^{\frac{1}{n}}$ and that the concavity is equal to m/n, *sensu stricto* Flint (1974). In this way,

if we can estimate m/n, we can measure the value of $\left(\frac{u}{K}\right)^{\frac{1}{n}}$ and relate this to either changes in relative rock uplift rate or bedrock erodibility. An estimate of the concavity index from slope-area analysis would also be equivalent to the m/n. However, slope-area analysis can magnify the errors associated with the noise inherent in Digital Elevation Model (DEM) data sets, making it unsuitable for large topographic analyses made possible by the availability of DEM data and advances in computing (Perron & Royden, 2013; Roberts et al., 2012; Smith et al., 2022).

1.2. Constraining m/n With the Integral Approach

The integral approach provides an alternative method to extract river network parameters from DEMs that is less sensitive to noise (Harkins et al., 2007; Perron & Royden, 2013; Royden et al., 2000). This is because it works directly with elevation data, as opposed to slope data that amplifies noise in an elevation data set (Mudd, Clubb, Gailleton, & Hurst, 2018). To work with elevations, and not slopes, we can recast Equation 3 as

$$\frac{dz}{dx} = \left(\frac{u}{K}\right)^{\frac{1}{n}} A^{-\frac{m}{n}}. \tag{4}$$

where z is the elevation, and x is the distance along the channel from the baselevel, x_b. Integrating Equation 4 provides the elevation of a point in the river network as an integral of downstream variables,

$$z(x) = z(x_b) + \int_{x_b}^{x} \left(\frac{u(x')}{K(x')}\right)^{\frac{1}{n}} A(x')^{-\frac{m}{n}}\, dx', \tag{5}$$

where u, K, and A may all vary with position. If channel steepness index, or $\left(\frac{u}{K}\right)^{\frac{1}{n}}$, is assumed to be spatially invariant, then,

$$z(x) = z(x_b) + \left(\frac{u}{K}\right)^{\frac{1}{n}} \int_{x_b}^{x} \frac{dx'}{A(x')^{\frac{m}{n}}}. \tag{6}$$

Here we have an expression for the elevation that can also be used to calculate the channel steepness index. However, it is conventional to introduce a reference drainage area A_0, which allows us to keep the units of the integrand in unit length. Hence, the integrand is defined as,

$$\chi = \int_{x_b}^{x} \left(\frac{A_0}{A(x')}\right)^{\frac{m}{n}} dx', \tag{7}$$

which is substituted into Equation 6 to give the elevation as

$$z(x) = z(x_b) + \left(\frac{u}{K{A_0}^m}\right)^{\frac{1}{n}} \chi. \tag{8}$$

As Equation 8 is a straight line equation of the form $y = c + mx$, where y and x are elevation and χ respectively, we can see that the gradient, m, is equal to the unknown parameter $\left(\frac{u}{K{A_0}^m}\right)^{\frac{1}{n}}$. This quantity is defined as u^* for simplicity and is the normalized relative rock uplift rate. In turn, any suitable regression through a χ-elevation data set can be used to extract u^*.

The χ values of a river network can be calculated through numerical integration. An example of how this can be done is with the TopoToolbox function *chitransform* (Schwanghart & Scherler, 2014), which calculates the cumulative integral of $\left(\frac{A_0}{A(x')}\right)^{\frac{m}{n}}$ with the trapezoidal method. To do this, however, we must know or estimate a value for m/n. A methodology to constrain m/n is possible using the χ-transformation itself, as shown in Figure 1, provided the river network experiences a specific set of conditions.

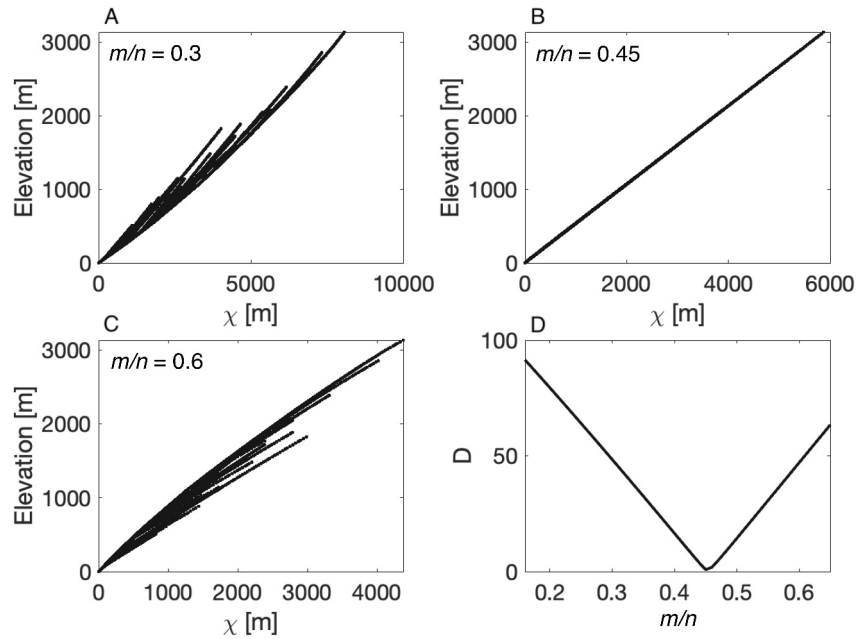

Figure 1. (a–c) χ-plots of a synthetic river profile created by performing the χ transformation of that river profile at different values for the concavity index. The synthetic river profile that these χ-plots are based on was created using the FastScape algorithm, where the rock uplift rate and erodibility were spatially invariable, and the concavity index value was 0.45. In panel (b), we see that the river profile collapses onto a line, as the trunk stream and tributaries are collinear when the correct value for the concavity index is used to perform the χ transformation. (d) A curve of disorder, D, versus concavity index for the simulated profile. The value at which D is at a minimum is 0.45, the value which was used to create the profile. This demonstrates the efficacy of this methodology for recovering the concavity index, provided channel steepness is spatially invariant.

If a river network is in steady state with a uniform u^* value, all parts of the network should have the same channel steepness index, and points on the network with similar elevations will also have similar χ values (Perron & Royden, 2013). When performing the χ transformation with the correct value of m/n, data pairs representing the trunk stream and the tributaries will be collinear, and collapse onto the same straight line (Figure 1b). However, at different values of m/n, the tributaries will not collapse onto the same line as the trunk stream (Equation 8, Figures 1a and 1c). We can use this principle to estimate the m/n value of a river network. This is done by finding the m/n value which minimizes the variability in a χ-elevation data set, which can be quantified with a disorder metric (Goren et al., 2014; Hergarten et al., 2016; Mudd et al., 2014; Perron & Royden, 2013). Here, we show the disorder metric as defined by Hergarten et al. (2016), but other methodologies use similar principles (e.g., Goren et al., 2014; Mudd et al., 2014; Perron & Royden, 2013).

In Figure 1, we simulate a steady state river network using the FastScape algorithm (Braun & Willett, 2013). The network has been created using a constant erodibility value, a temporally and spatially invariant rock uplift rate, and an m/n value of 0.45. To determine the m/n value from the χ-elevation data, we first perform the χ transformation at different values of m/n, as demonstrated in panels A, B and C. At each value of m/n, we calculate the disorder, D, introduced by Hergarten et al. (2016). This is done by first sorting the river nodes in ascending order of elevation and then calculating the sum of the absolute differences between the χ-values of adjacent nodes such that the sum of the differences, ψ, can be expressed as

$$\psi = \sum_{i=1}^{n} |\chi_{i+1} - \chi_i|. \tag{9}$$

As the absolute values of χ differ depending on the value of m/n used, it is necessary to rescale S to the maximum value of χ in the river network at each value of m/n to prevent bias toward values of m/n that produce small overall values of χ. Doing this, we arrive at the calculation of the disorder, D, where

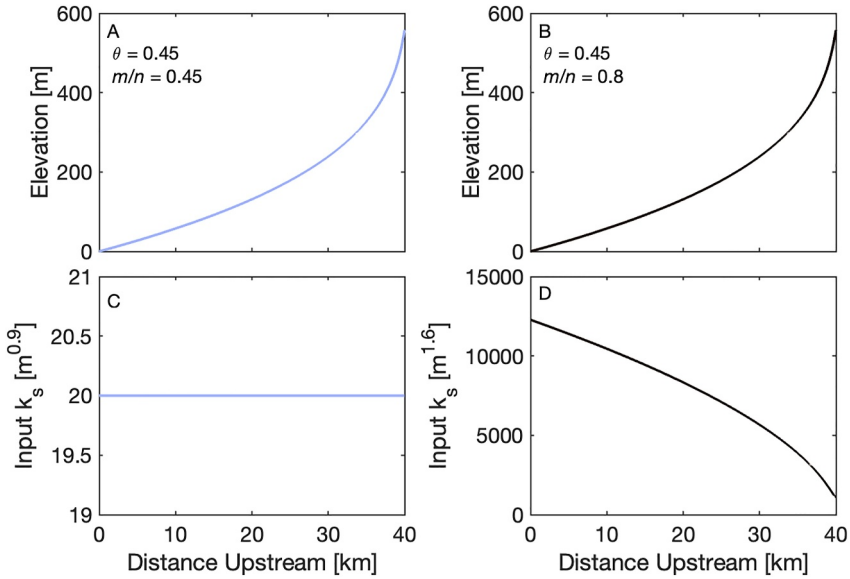

Figure 2. Two identical river profiles, with different values of *m/n*. (a) A river network created with a spatially invariant channel steepness index (c). This profile has a concavity index equivalent to the *m/n*. (b) A profile created with an *m/n* of 0.8, and a decreasing gradient in channel steepness index (d), which makes a profile with a concavity index of 0.45. (c) The input channel steepness index used to create (a). (d). The input channel steepness index used to create (b). River profiles are in steady state, such that the rock uplift and erosion rates are balanced. As the profiles are created using channel steepness index, changes to channel steepness index could represent changing rock uplift or erodibility.

$$D = \frac{\psi - \chi_{\max}}{\chi_{\max}}. \tag{10}$$

If the trunk stream and tributaries are perfectly collapsible, the value of D should be 0. As expected, when calculating D across a range of *m/n* values for the simulated river network in Figure 1, the value closest to 0 is the value that was used to simulate the network, 0.45. Note that the value is not exactly 0 likely due to numerical diffusion. The disorder methodology reliably infers the correct value of *m/n* when there is no spatial variation in rock uplift and erodibility. Under these conditions, the concavity index of the river provides an accurate estimate of the *m/n* ratio.

Provided a river network has experienced spatially invariant channel steepness index values, no matter the temporal variation in channel steepness index, the above-described methodology and similar methodologies (e.g., Goren et al., 2014; Mudd et al., 2014) all accurately recover the correct *m/n* value (Supporting Information S1). However, when spatial variation in the channel steepness index is introduced, this is no longer the case.

1.3. The Influence of Spatial Gradients on Estimates of *m/n* and Concavity

Spatial gradients in rock uplift and erodibility are present in almost every setting on Earth, at a wide range of spatial scales. For a mountain range experiencing rock uplift along a normal fault, the rock uplift rate decreases away from the fault (Anders et al., 1993; Armstrong et al., 2003; Buck, 1988). For topography being created by folding, the rock uplift rate is highest on the axial plane of the fold, and decreases away from the center (Bufe et al., 2016; Lavé & Avouac, 2000). Gradients in precipitation caused by orographic effects can translate to gradients in erodibility (Adams et al., 2020; Han et al., 2015; Leonard & Whipple, 2021; Roe et al., 2002), along with a number of other factors such as weathering regime and sediment production that vary within single catchments (Riebe et al., 2015). This is problematic as gradients in channel steepness index (as defined in Equation 3) along the course of a river network create river long profiles that appear to have constant channel steepness index but are actually experiencing spatial variation. This is demonstrated in Figure 2.

In Figure 2, two identical synthetic profiles have been created using different values for the *m/n*. The elevations of these profiles were calculated using Equation 5, and the channel steepness index functions shown in Figures 2c

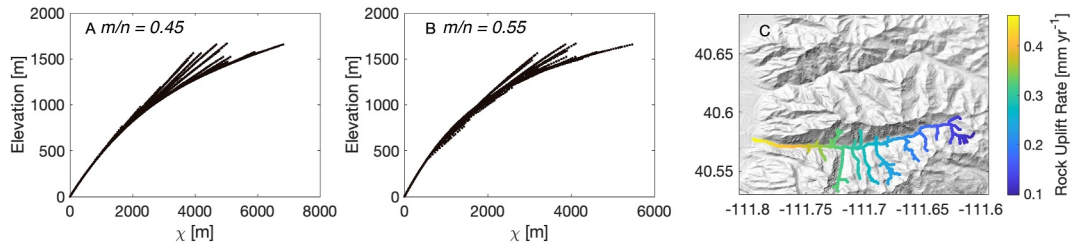

Figure 3. (a) A χ-plot of the Little Cottonwood Canyon river network, with synthetic elevations that were simulated using the FastScape algorithm, and the gradient in rock uplift rate shown in (c). As the tributaries run perpendicular to the gradient in rock uplift, they sample a constant u^* value such that the χ-elevation relationship departs from the χ-elevation relationship of the trunk stream. This χ-plot is created with the true value for m/n, that is, the m/n that was used to simulate the elevations. (b) A χ-plot of the same network is obtained, but the χ-transformation is performed using the value of m/n that minimizes the disorder between nodes (Hergarten et al., 2016). The result is that the measured m/n is different from the true m/n. The value of m/n used to simulate the river network is 0.45, but the recovered value of m/n from the method of Hergarten et al. (2016) is 0.55. (c) The river network used to create the χ-plots of (a and b). There is a gradient in the rock uplift rate that interacts with different portions of the network in different ways.

and 2d. In profile Figure 2a, the value of m/n is equivalent to the concavity, and the channel steepness index values it experiences are spatially invariant. However, profile Figure 2b has experienced a decreasing gradient of channel steepness index. Even though a greater m/n ratio is used, the concavity index is identical to that of profile Figure 2a. If we were to perform slope-area analysis on these two profiles, they would yield the same estimated values of the channel steepness index and the concavity index. In this way, if a channel experiences spatial variation in relative rock uplift rate, the channel steepness index and concavity index as defined by Flint contain no information regarding either rock uplift or erodibility. This is not useful from the perspective of tectonic geomorphology, and is also important to consider if one wishes to use an estimate of the concavity index as the value of m/n.

Spatial variation causes Flint's concavity index to deviate from the best-fitting m/n of a river network, but it also causes issues for the χ-based approaches to estimate m/n that have been described in Section 1.2 and are based on an assumption of spatially uniform u^*. This is because spatial variation can cause the trunk stream and tributaries of a river network to experience different u^* values, which means it is inappropriate to minimize the variance between them. Consider the example in Figure 3. Here, we have simulated the elevations of the Little Cottonwood Canyon river network that drains the Wasatch Range in Utah. The network has a geometry suitable for evaluating the phenomenon described above as it has a trunk stream that runs E-W, and tributaries that run perpendicular to the trunk in a N-S direction. River network elevations were simulated at an m/n value of 0.45 using the FastScape algorithm (Braun & Willett, 2013). We impose a gradient in the rock uplift rate such that rock uplift rate values are greater close to the base level and lower in the headwaters (Figure 3c). The χ-elevation relationship at the correct value of m/n would show a trunk stream with a decreasing slope from the baselevel toward the headwaters, reflecting the gradient in rock uplift rate and thus the channel steepness index (Figure 3b). However, as the tributaries run almost perpendicular to the trunk stream, the change in rock uplift rate that they experience along their length is much less significant (almost negligible) than the change experienced by the trunk stream. The χ-elevation relationship for the tributaries would therefore be almost linear and the slope would be equal to the slope of the χ-elevation relationship of the trunk stream at the location of the confluence. As such, the tributaries depart from the χ-elevation relationship of the trunk stream and plot above the trunk channel at the true value of m/n (Figure 3a). It is also important to note that this is simply due to spatial gradients in channel steepness, and not due to drainage divide migration (Willett et al., 2014).

If we use the methodology described in Section 1.2 or similar methodologies that require the tributaries and trunk stream to experience spatially uniform normalized rock uplift, the measured m/n value will not be the m/n value that best describes the data in a stream power model framework. This is because the disorder metric will attempt to find a value for the m/n that prevents the tributaries departing from the χ-elevation relationship of the trunk stream (Figure 3b). In the example in Figure 3, the estimated m/n is higher than the m/n used to simulate the network (the network was simulated with a m/n of 0.45, but the estimated m/n of Figure 3b is 0.55). This can have serious consequences for measured values of the channel steepness index, as shown by Gailleton et al. (2021).

In summary, existing methodologies to estimate the m/n ratio required for topographic analysis rely on the assumption of spatially invariant rock uplift and erodibility (Goren et al., 2014; Harkins et al., 2007; Mudd et al., 2014; Perron & Royden, 2013; Wobus et al., 2006). The estimated m/n value, or concavity, is then used to calculate spatial variations in the channel steepness index. This is clearly problematic. To prevent this, we present a methodology that can account for spatial variation in channel steepness on a river network, allowing us to utilize information contained in the tributaries to accurately estimate m/n and the channel steepness index.

2. Methods

In this study, we assess how spatial gradients in the channel steepness index influence the estimation of m/n using a synthetic data set created with a known m/n and real examples from the Olympic Mountains and Siwalik Hills. We also develop a new methodology to constrain m/n that is unaffected by spatial gradients in the channel steepness index. In this section, we describe our new methodology to constrain m/n (Section 2.1), and how we create synthetic landscapes (Section 2.2).

2.1. A Topographic Inversion for m/n

Our methodology estimates m/n using a topographic inversion similar to that described by Smith et al. (2022). The methodology is based on a similar principle to the χ-disorder methods in that we repeat the χ-transformation across a range of values for the m/n, and observe which value of the m/n produces the best fit to the data. The basis of our methodology comes from a linear inversion that calculates spatially variable u^* across a region. Note that as we are solving for u^*, we do not need to specify a value of n, and can find the optimal m/n through linear inversion even when n does not equal one.

To define the u^* of a region, we discretize the region onto a grid which defines the number of u^* values being solved for. We then use Equation 5 to describe the elevation of each river node as a summation of the differences in χ between river nodes downstream, and the channel steepness index values at each of those downstream nodes. This can be done using the following equation. Take three river nodes, i, j, k, where k is upstream from j, which is upstream from i, which is upstream from the baselevel (at 0 m). If i, j and k have u^* values u_1^*, u_2^* and u_3^* respectively, we can write the elevation of point k as,

$$\begin{bmatrix}(\chi_i - 0) & (\chi_j - \chi_i) & (\chi_k - \chi_j)\end{bmatrix}\begin{bmatrix}u_1^*\\ u_2^*\\ u_3^*\end{bmatrix} = z_k, \tag{11}$$

where χ_i is the χ value of river node i. We can then write this summation for all the river nodes in our drainage network, and combine the equations into the matrix-vector product such that,

$$\mathbf{Au} = \mathbf{z}. \tag{12}$$

Here, $\mathbf{A}$ is an $N \times q$ matrix, where N is the number of nodes in the river network, and q is the number of u^* parameters defined by the grid. This grid is a discretization of space with pixel sizes larger than the DEM resolution. Each river node from the DEM grid within a cell defining a u^* parameter is thus forced to experience the same u^* value. As such, there are typically more river nodes, N, than u^* parameters, q. Each row of the $\mathbf{A}$ matrix represents 1 river node and $\mathbf{u}$ is a vector of length q, where each row represents a cell on the discretized u^* grid corresponding to a u^* parameter. In the case where multiple river nodes are located in the same u^* cell, the downstream differences in χ of these nodes are added together.

To solve for the channel steepness index values, we must calculate the inverse of Equation 12. However, the inverse of Equation 12 is a mixed-determined system (Menke, 2012). Some u^* parameters may be constrained by one or more river nodes, but others may not be constrained by any depending on how the river network intersects with the u^* grid. Thus, as the problem is ill-posed, we must introduce some form of regularization (Parker, 1994). This is done by using a Laplacian operator as a roughness constraint that can be used to penalize solutions that have large differences in u^* close together in space. For the u^* value at coordinates i, j on the grid, the roughness around the cell is described as

$$\nabla^2 u^*_{i,j} = 4 \times u^*_{i,j} - u^*_{i+1,j} - u^*_{i-1,j} - u^*_{i,j+1} - u^*_{i,j-1}. \quad (13)$$

We incorporate this term into our system of equations in Equation 12 by creating a new matrix, **W**, that has the dimensions $q \times q$, and combining it to the base of the **A** matrix. Each row of this matrix has 5 non-zero entries to calculate the roughness around one u^* parameter. By setting **W u** equal to a vector of zeros in our inverse scheme, we force the solution to minimize the roughness around each u^* parameter, and arrive at the following,

$$\begin{pmatrix} \mathbf{A} \\ \alpha \mathbf{W} \end{pmatrix} \mathbf{u} = \begin{pmatrix} \mathbf{z} \\ \mathbf{0} \end{pmatrix}, \quad (14)$$

where **0** is a vector of 0s, of length q. This form of Tikhonov regularization (Tikhonov & Arsenin, 1977) has been used in similar river network inversions (e.g., Fox et al., 2024), and allows us to solve this system with a linear least squares approach. Note that we also include a scalar value, α, that controls the importance of smoothness to the solution. In this way, the least squares approach will find a solution that balances the fit to the data and the model roughness by minimizing the misfit, ϕ, defined as,

$$\phi = \|\mathbf{A}\mathbf{u} - \mathbf{z}\|^2 + \alpha^2 \|\mathbf{W}\mathbf{u} - \mathbf{0}\|^2. \quad (15)$$

Here, we see that when α is larger, the roughness values contribute more heavily to the misfit, so the solution is forced to be smooth to minimize this. When α is decreased, the opposite is true, and the fit to the data is prioritized. To choose an appropriate value for α, we use an L-curve, a plot of the norm of the solution vector (**u**) and the norm of the residuals (**Au** − **z**) (Hansen, 1992). This allows us to choose a value for α that balances the trade-off between smoothness and a good fit to the data. Following Hansen (1992), we choose a solution that comes from the "elbow" of the L-curve (Figure S1 in Supporting Information S1).

The inversion scheme set out above is able to recover spatially variable u^* values from the χ values and elevation data of a river network. We can then use the inferred u^* parameters to predict the elevations of the network, and infer the value of *m/n* in a region. This is done by performing the following routine for a range of different values of *m/n*. First, the χ values are calculated using the given value of *m/n*. Next, we build the **A** matrix using these χ values. We perform the inversion outlined above to infer the spatially variable u^* values, and then multiply the inferred **u** vector by the **A** matrix to predict the elevations of the river network. Finally, we calculate the misfit between the predicted and the real elevations. Once this has been performed for a range of *m/n* values, we can plot a graph of *m/n* versus misfit. In the same way that the *m/n* value that minimizes the disorder metric in the χ-disorder methods is the one used for analysis, the value of the *m/n* that minimizes the misfit here is the best fitting *m/n* value for the study region. For clarity, this workflow is outlined in Figure 4. One further consideration we make is to normalize the χ-values calculated for each value of the *m/n* to the same arbitrary number, in this case 10,000. This ensures that the smoothing parameter, α, has the same weighting in each solution. For the sake of simplicity, we have normalized the χ-values to the same value in all of our analysis, allowing us to use the value of α justified from an L-curve from the Siwalik example (Figure S1 in Supporting Information S1) for each analysis.

2.2. Creating Synthetic Landscapes

We use Equation 12 as the basis for creating synthetic landscapes with known gradients in the channel steepness index and a known value of *m/n*. First, we use *TopoToolbox* (Schwanghart & Scherler, 2014) to extract the drainage network from a DEM. For our analysis, we use the commonly used 30 m Shuttle Radar Topography Mission DEM data set (Farr et al., 2007) for the Uinta Mountains, Utah. The drainage network is extracted using a threshold area for channel initiation of 1 km^2. We perform the χ-transformation at an *m/n* value of 0.45, build the **A** matrix in Equation 12 and then define a **u** vector that describes a grid of u^* parameters that have a gradient from North to South. By multiplying **A** by **u**, we create a steady-state landscape that has experienced a gradient of channel steepness index and has an *m/n* of 0.45. Although the simulated network may not perfectly reflect a real-life landscape, owing to variation in elevations across drainage divides with different χ-values, this does not influence our analysis. Instead, using a real landscape is advantageous as it ensures that the drainage network is representative of a real drainage network. The choice of the Uintas over other regions is also advantageous as the rivers draining the Uintas flow away from the center of the range, such that some rivers drain to the North, some to

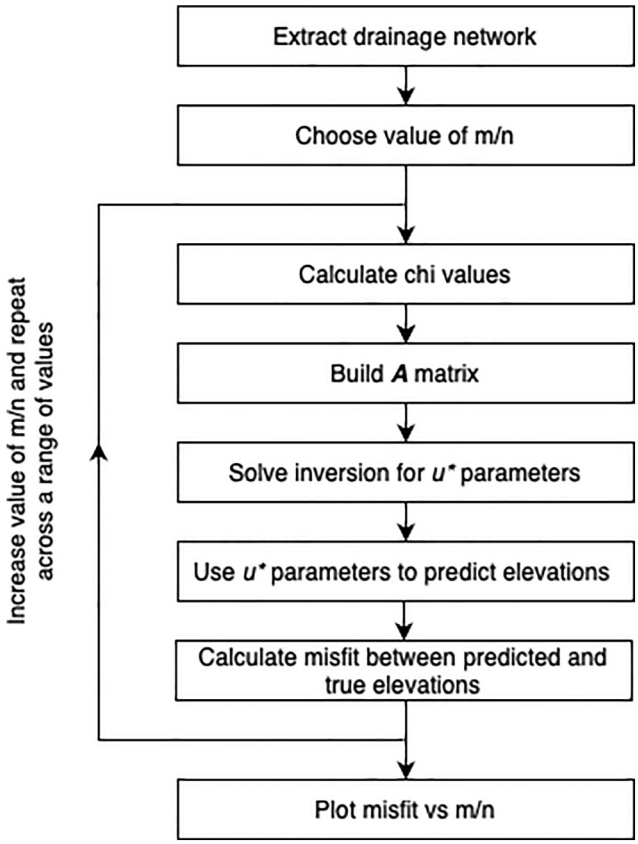

Figure 4. A flow chart outlining our methodology for determining the concavity index from a topographic inversion.

the East and some to the South. This allows us to impose a gradient in channel steepness from North to South and examine the combination of scenarios (i.e., networks flowing parallel and perpendicular to a gradient of channel steepness index). It is important to note that we only use the upstream drainage area information of the Uinta river networks; the elevation data of these networks are totally synthetic.

3. Results

We test a number of existing methodologies and our new methodology to infer *m/n* on synthetic and real-life landscapes. The focus of this work is to highlight the importance of spatial gradients in factors influencing channel steepness index on river networks and how this is manifested in the metrics commonly used in geomorphic studies. However, to ensure that our new methodology is robust, we have also tested it in a number of other scenarios, such as a temporal change in the relative rock uplift rate, and a step change in the spatial distribution of relative rock uplift. Our new methodology accurately estimates the correct value of *m/n* in these additional tests, which are available in Supporting Information S1. In the following section, we focus on how gradients in relative rock uplift rate influence estimates of the concavity index and *m/n*.

3.1. Synthetic River Network

3.1.1. χ-Disorder Methodology

The *u** values (here reported as the more familiar channel steepness index) used to create the synthetic landscape are shown in Figure 5a. The values of the channel steepness index increase from the north to the south, allowing us to examine how gradients in this parameter influence *m/n* estimates. As previously mentioned, as the rivers flow in different directions, they are influenced by different gradients. Those flowing to the north experience a decrease in the channel steepness index as they flow downstream, whereas the opposite is true for the rivers flowing to the south. As the rivers in this landscape were created with an *m/n* value of 0.45, any deviation from this value is due to the influence of spatial gradients.

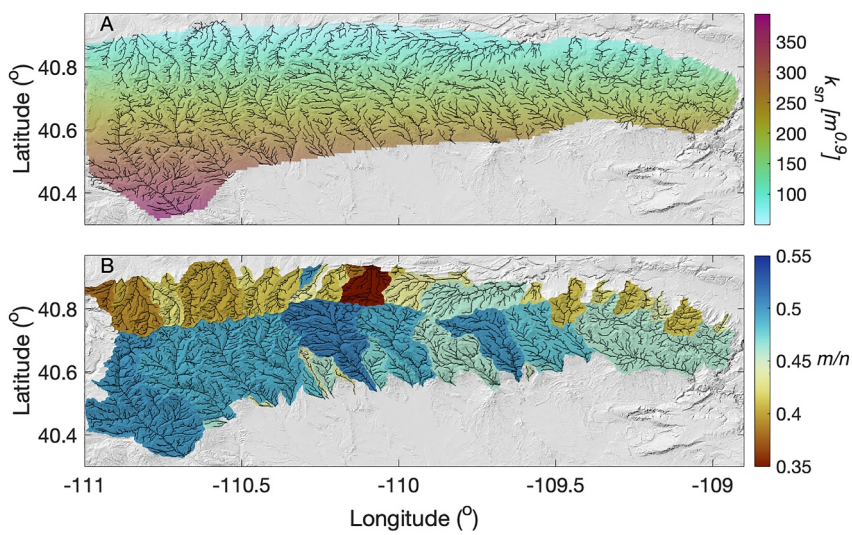

Figure 5. (a) The map of channel steepness index used to create the synthetic river networks. (b) The inferred *m/n* values of 50 river networks, as measured using the methodology of Hergarten et al. (2016).

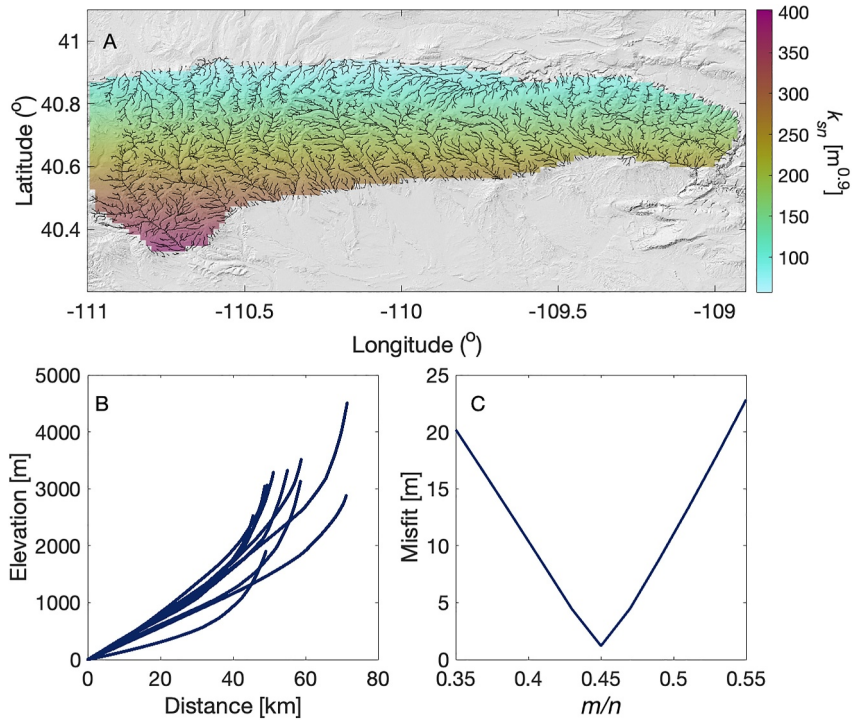

Figure 6. (a) The inferred channel steepness index map from the inversion at the best fit *m/n* of 0.45. (b) Ten predicted river profiles using our inversion parameters (navy blue) overlain on the true profiles (pale blue). The true profiles are not visible as the fit to the data is nearly perfect. Note that the profiles have different apparent concavity indexes, similar to Figure 1, due to the varying influence of the gradient in the channel steepness index depending on which direction the rivers flow. (c) A curve of the misfit between observed and predicted river profiles versus the *m/n*. The minimum misfit value occurs at an *m/n* value of 0.45, the true value of the synthetic landscape.

In Figure 5b, we show the inferred *m/n* values of 50 catchments across our synthetic landscape, as measured by the methodology of Hergarten et al. (2016). The inferred *m/n* values vary systematically depending on the dominant direction the river network flows with respect to the gradient. Networks that drain to the north, which encounter a decreasing gradient in channel steepness index as they flow downstream, have systematically lower measured *m/n* values compared to the true value. The rivers that drain to the south do the opposite; they flow toward an increasing gradient in the channel steepness index, and have higher *m/n* values than the true value. This signal is due to the phenomenon outlined in Section 1.3, where we show that, as tributaries and the trunk stream of a river network intersect gradients in channel steepness index differently, they have different gradients on a χ-plot at the true value of *m/n*. Therefore, any attempt to collapse the χ-elevation data where there is a spatial gradient invariably results in an incorrect estimate of *m/n*. Even when the difference in channel steepness index from the baselevel to the headwaters is relatively small (less than 50 m$^{0.9}$), as it is for some of the rivers draining to the north, this gradient still has an appreciable effect on the measured values of *m/n*.

Rivers that flow in an E-W direction are influenced least by the gradient, as they flow over relatively constant channel steepness index values. As such, these networks have estimated *m/n* values very similar to the true value. A good example of such a network is the easternmost network, which has a pale blue color corresponding to an *m/n* value of 0.46.

3.1.2. Inverse Method for Constraining *m/n*

Using the inverse method to constrain *m/n*, we must first recover the channel steepness index or u^* values. As opposed to DEM data, which contains noise and artifacts, and real landscapes, which contain geomorphic noise such as vegetation and landslides, there is no such noise in the synthetic network. This means that the inferred channel steepness index map is very similar to the actual channel steepness index map when using the correct value of *m/n* (Figure 6a). The small differences in the estimated values of the channel steepness index and the true

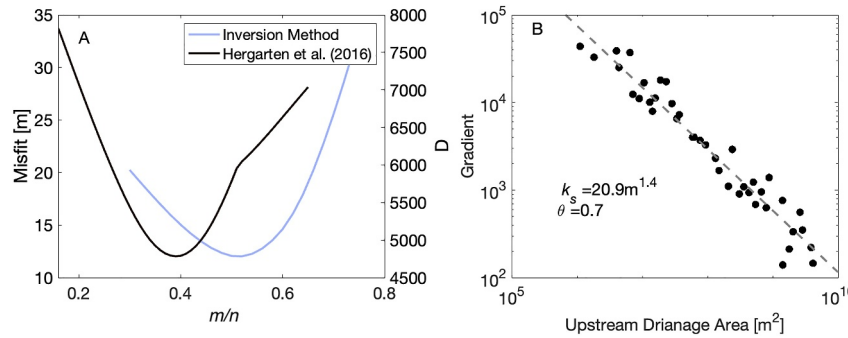

Figure 7. Estimates of the concavity index and *m/n* for the Clearwater river using three different methodologies. (a) The χ-disorder method and our method are shown together, as they both produce curves in which the minimum value of either misfit or disorder indicates the value of the *m/n*. The χ-disorder method estimates an *m/n* of 0.39, and our method estimates an *m/n* value of 0.51. (b) The Slope-Area methodology to infer the concavity index. The inferred value of the concavity is 0.7, much greater than the *m/n* estimated using the other methods.

values are due to the inclusion of the smoothness constraint in our inversion. As there is no noise, the value of the smoothness parameter is not important as long as it allows us to infer a stable solution. Given that the inferred channel steepness index values are so similar to the actual channel steepness index values, the predicted river networks are almost identical to the actual river networks (Figure 6b). However, when the value of *m/n* used in the inversion deviates from the true value of *m/n*, the misfit between the predicted and synthetic networks becomes greater. The result is that a plot of misfit versus *m/n* produces a curve with a minimum at the true value (Figure 6c). The trough of this curve falls at 0.45, demonstrating the ability of the methodology to recover an accurate estimate of *m/n*.

3.2. The Clearwater Catchment, Olympic Mountains

The Olympic Mountains are uplifted due to deformation within the accretionary wedge of the Cascadia subduction zone (Brandon et al., 1998). The Clearwater River is a tributary of the Queets River, one of the three major rivers draining the range. As the Clearwater has been shown to be in steady state (Pazzaglia & Brandon, 2001), and the exhumation rate within the clearwater and surrounding region is well constrained by thermochronometry (Brandon et al., 1998; Michel et al., 2018), it represents an ideal study area to evaluate how estimated *m/n* values can differ in natural settings. Although there is a slight increase in precipitation from the base-level of the Clearwater (here, taken as the confluence with the Queets river) to the headwaters (Prism Climate Group, 2014), the dominant process that should influence the channel steepness index is a 3-fold increase in the rock uplift rate from baselevel to the headwaters, as evidenced by long-term thermochronometric data and modeling (Brandon et al., 1998; Michel et al., 2018).

3.2.1. Measuring *m/n* of the Clearwater River

We use three different methodologies to estimate the *m/n* of the Clearwater river (Figure 7). The first is binned slope-area analysis, which uses an assumption of spatially invariant channel steepness index to estimate the concavity index which would also be assumed to be the *m/n* value in the catchment (Wobus et al., 2006). The binned slope area analysis was performed using the *slopearea* function in TopoToolbox (Schwanghart & Scherler, 2014), where the slope and upstream drainage area data were separated into 50 bins, before being log-transformed and having a linear model fit through it. The second is the χ-disorder method described in Section 1.2, which also assumes spatially invariant channel steepness index but estimates the *m/n* ratio directly (Hergarten et al., 2016). Finally, we use the method presented here based on a topographic inversion, which allows the channel steepness index to vary and estimates the *m/n.* The inversion is performed using a grid-size of 2 km. All three methodologies estimate different *m/n* values for the Clearwater. The binned slope-area method estimates a concavity index value, and as the slope-area data do not belie any gradient (the relationship appears linear), we would also assume an *m/n* of 0.7. This is much higher than typical values of *m/n* (0.4 <*m/n*> 0.6) used in similar tectonic settings (Kirby & Whipple, 2001, 2012; Snyder et al., 2000; Wobus et al., 2006). The other two methodologies, however, estimate values that are closer to those typical values for steady-state river networks.

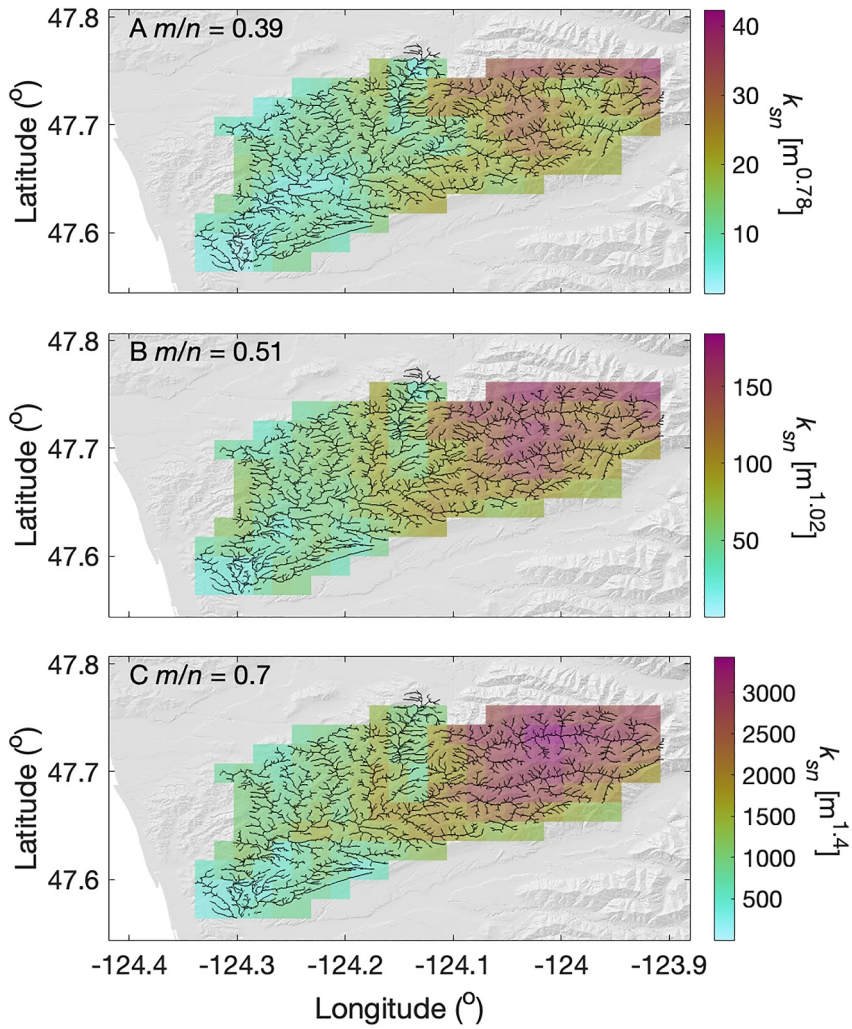

Figure 8. Channel Steepness index maps created at the three different values of the *m/n* inferred from three different methodologies.

The *m/n* estimated using the χ-disorder method is 0.39, whereas the value estimated by our methodology is 0.51. This result is what is expected given the observations from the synthetic data set. When a river flows over a decreasing gradient of channel steepness index, the long-profile of that river has a greater concavity index than the value of *m/n* (the opposite scenario to Figure 2b). This is reflected in the value of the concavity index estimated using the slope-area methodology. However, when *m/n* is estimated using the χ-disorder method, a decreasing gradient results in a lower estimation of the concavity index owing to the influence of tributaries (Figures 3 and 5). Our methodology on the other hand estimates an *m/n* in between these two values.

3.2.2. Influence of *m/n* on Channel Steepness Index

The different *m/n* values inferred from these methodologies have demonstrable effects on channel steepness index maps of the Clearwater catchment, and the interpretations that can be made from them. In Figure 8, we show three channel steepness index maps of the clearwater catchment, created with the three estimated values of *m/n*. To calculate channel steepness index values, we use our inverse scheme for u^*, but report values as the more familiar channel steepness index. We normalize the χ-values as described in Section 2.1, such that the smoothness constraints have the same influence on each solution. In this way, the value of the *m/n* is the only parameter influencing differences in the normalized channel steepness index maps.

One obvious difference between the inferred channel steepness index maps is the absolute values of the inferred channel steepness index, which change by orders of magnitude at different values of *m/n*. However, another key difference between the maps is the magnitude of the gradient in the channel steepness index inferred from the baselevel to the headwaters. At an *m/n* value of 0.39, the values of the channel steepness index near the baselevel are approximately 10 $m^{0.78}$, increasing to average values of 20–25 $m^{0.78}$ upstream. At a value of 0.51, channel steepness index values similarly increase, but at this value they increase from approximately 50 $m^{1.02}$–150 $m^{1.02}$. At a concavity index value of 0.7, the magnitude of this gradient is much higher, with channel steepness index values changing upstream from approximately 500 $m^{1.4}$ to 3,000 $m^{1.4}$. Thus, at an *m/n* value of 0.39, channel steepness index values double from the baselevel to the headwaters, whereas they triple along the same area in the map created using an *m/n* 0.51 and sextuple according to the map created using an *m/n* of 0.7. The value of *m/n* therefore changes not only the absolute values of the channel steepness index but the magnitude of the inferred gradient in the channel steepness index. This phenomenon has been reported previously (Figure 14 in Gailleton et al. (2021)).

3.3. The Mohand Range, Siwalik Hills

The Siwalik Hills represent the active deformation front of the Himalaya, forming due to fold growth as a result of thrusting along the Himalayan Frontal Thrust (Gansser, 1964; Hurtrez et al., 1999; Lavé & Avouac, 2000; Yeats & Lillie, 1991). As the active front of the largest mountain range in the world, studies focused on the Siwalik Hills have greatly developed our understanding of orogen growth (Avouac, 2003; Burgess et al., 2012; Hurtrez et al., 1999; Kirby & Whipple, 2001, 2012; Lavé & Avouac, 2000; Yeats & Thakur, 2008; Yin, 2006). The active and recent nature of uplift in the Siwalik Hills also causes the signatures of tectonic processes to be clearly imparted on river networks that drain the range. As such, many seminal studies from both the perspective of Himalayan deformation, and fluvial geomorphology, have focused on the Siwalik Hills (Avouac, 2003; Kirby & Whipple, 2001; Lavé & Avouac, 2000, 2001; Wobus et al., 2006).

The Mohand Range is one of the ranges that makes up the Siwalik Hills, uplifted by the growth of the Mohand anticline. There is a debate as to whether the structure is a fault-bend fold or a fault-propagation fold (Barnes et al., 2011; Powers et al., 1998; Srivastava et al., 2016, 2018; Wesnousky et al., 1999), which has important implications for the distribution of rock uplift across the range. In both cases, the rock uplift rate should decrease from the range front in the southwest to the northeast. We should: (a) be able to recover this signal from the river networks and (b) observe whether this gradient influences calculations of *m/n*. The spatial gradient in rock uplift is, however, confounded by a lithological contact, which separates the stronger Middle Siwaliks in the southwest from the softer unconsolidated Upper Siwaliks to the northeast (Allen et al., 2013; Barnes et al., 2011; Kirby & Whipple, 2012). The effect of this boundary is to create the same gradient in the channel steepness index as expected from the fault growth, with higher values in the southwest.

3.3.1. χ-Disorder Methodology

A map of *m/n*, as measured using the methodology of Hergarten et al. (2016), was created by Wahyudi et al. (2021), and has been recreated here for 100 rivers draining the Mohand Range (Figure 9). There is systematic variation in measured *m/n*, similar to the synthetic example, suggesting a gradient in channel steepness index across the range is present. The rivers that drain the southwestern flank of the range have higher measured *m/n* values on average than the rivers draining the northeast. For the rivers draining the southwest, the higher values of *m/n* could be explained by the increase in the channel steepness index due to the increased rock strength from northeast to southwest (Figure 10). Providing further evidence for this is the observation that the rivers on the southwestern flank that have lower values of *m/n* (around 78° Longitude) do not sample this change in rock strength, as the Bhimgoda thrust reverses the lithological boundary (Figure 10; Raiverman et al., 1990; Wesnousky et al., 1999). However, with no change in lithology influencing the rivers draining the northeastern flank, it is difficult to explain why the measured *m/n* of these rivers is so low without the existence of a spatial gradient in channel steepness index.

3.3.2. Constraining *m/n* and Normalized Channel Steepness Index With an Inversion

As shown in Figure 9, the *m/n* of individual basins around the Mohand Range appear to be different when measured using a χ-disorder method (Hergarten et al., 2016). The *m/n* of rivers draining the southwestern flank of

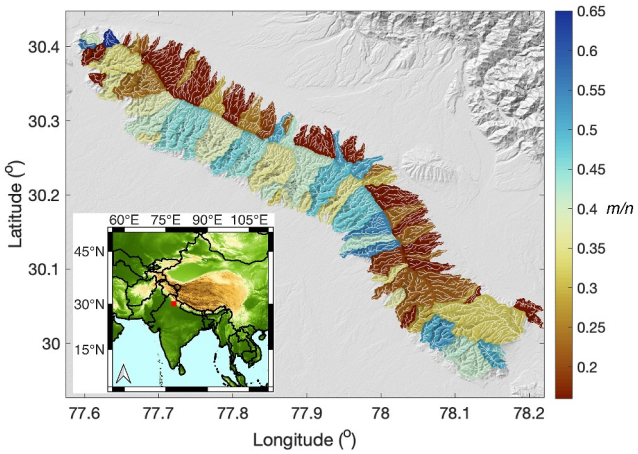

Figure 9. A map of *m/n* for 100 catchments of the Mohand Range calculated using the method of Hergarten et al. (2016). The average value of *m/n* if we simply take the mean of the 100 catchments is 0.29, and if weighted by drainage basin area is 0.32. This is similar to the value inferred from the inversion method, though it is not clear whether taking an average of these values has any physical meaning. Inset map shows a regional map with the Mohand Range signified by a red square.

the Mohand range has also been measured as different along different sections of the same trunk streams (Kirby & Whipple, 2012). Using the measured values of *m/n* to calculate the channel steepness index would make the comparison of channel steepness index values difficult, as the units and those values are heavily influenced by *m/n* (e.g., Figure 8). However, it is also difficult to determine a single value for the reference concavity index or *m/n* that should be used to calculate the normalized channel steepness index to facilitate comparison of channel steepness index values across the range. In the Mohand Range, a value of 0.45 has been used, as it can be linked to previous studies in the Siwaliks and Himalaya (Kirby & Whipple, 2001, 2012; Wahyudi et al., 2021). However, this estimate is based on a concavity index measurement (Kirby & Whipple, 2001), which requires spatially invariant rock uplift and erodibility to represent the *m/n*. As this assumption is not true in the Siwaliks, it is unlikely that the *m/n* value of 0.45 is the value that best describes the river networks. This would cause issues when calculating normalized channel steepness index values for the range (Gailleton et al., 2021).

We apply our methodology to the Mohand Range so that we can recover the best fitting value of *m/n* for the range, which can then be used to create a normalized channel steepness index map. In Figure 10c, the curve of misfit versus *m/n* derived from our inversion indicates that the best fitting value of the *m/n* is 0.31. This is lower than the concavity index value of 0.46 measured by Kirby and Whipple (2001) for the Siwaliks. The misfit curve has a slightly broader trough than the synthetic example, and this is likely due to the influence of noise in this real data set. The value of 0.31 has then been used to predict the elevations of 10 trunk streams from around the range (Figure 10b), which show a good fit to the real profiles, and to create a map of normalized channel steepness index (Figure 10a). The value of the smoothness constraint, α, used in the analysis was chosen from an L-curve (Supporting Information S1).

The normalized channel steepness index map picks out the lithological boundary between the Upper Siwaliks and the Lower/Middle Siwaliks, such that there are much higher values of channel steepness index on the southwestern flank of the range. However, there are also increased channel steepness index values at the drainage divide, which create a gradient in channel steepness index from high to low downstream along rivers draining the northeastern flank (Figure 10). The decreasing gradient from headwaters to baselevel is also present in the rivers draining to the southwest, but is imposed over the change in channel steepness index caused by lithology.

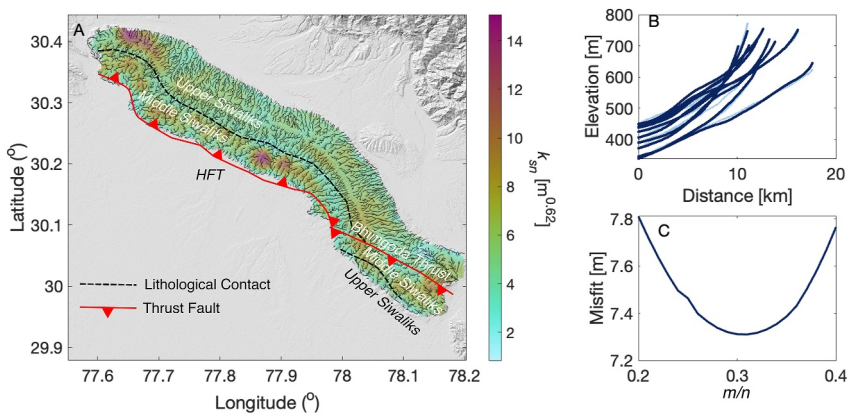

Figure 10. (a) A channel steepness index map of the Mohand Range, created using an *m/n* value of 0.31. Channel steepness is clearly influenced by lithology; however, there are also higher channel steepness index values at the drainage divide, such that all of the river networks, whether they drain the northeastern or southwestern flank, have a decreasing gradient in channel steepness index imposed on them. (b) The 10 largest trunk streams of the Mohand Range (light blue), and the predicted trunk streams from the channel steepness index values of (a). (c) The graph of misfit versus *m/n* using our inversion scheme. The best fitting *m/n* value is 0.31. HFT, Himalayan Frontal Fault.

Splitting the river networks draining the southwestern flank at the lithological boundary (where there is a rapid increase in channel steepness index), both sections sample a decreasing gradient in channel steepness index, despite the overall gradient appearing to increase downstream. The implications of this pattern are discussed later.

4. Discussion

4.1. What Causes Under or Over Prediction of *m/n*?

In Figure 2, we show how spatial gradients in the channel steepness index can cause rivers that have the different *m/n* values to have the same concavity indices. If the estimated concavity index value is conflated with the *m/n* value, there are important implications for estimated channel steepness index values. Furthermore, the methodology used to infer *m/n* can produce systematic variation in the estimated values of *m/n* if the relative rock uplift rate varies in space.

The river profile in Figure 2b is similar to the rivers draining to the south in our synthetic example (Figure 5) in that they all sample gradients of decreasing channel steepness index toward their headwaters. The profile in Figure 2b has a lower concavity than the *m/n* that created it. This would be reflected in the measured value of concavity using a slope-area methodology. On the other hand, in our synthetic example, the same pattern produces higher values of *m/n* measured using the χ-based method (Figures 5 and 7). This is because on a χ-plot, the gradient of the trunk stream of this river will decrease toward higher values of χ, but as the tributaries flow subperpendicular to the trunk stream, they do not experience a gradient in the channel steepness index. This is the scenario observed in Figure 3. The gradient of the tributary χ-elevation relationship is thus linear, and will be tangential to the trunk stream. The result is that the χ-plot of a river network experiencing a decreasing gradient to the headwaters, transformed with the correct *m/n* value, will have a curved trunk stream with tributaries extending above. In order to minimize the disorder of this network, the χ-transformation needs to decrease the gradient of the χ-elevation relationship of the tributaries, which can be achieved by performing the χ-transformation at larger values of *m/n* (Figure 1c). This explains why two different methodologies may infer different values for *m/n* for the same area, as typified in the Clearwater example. Here the gradient in channel steepness index increases toward the headwaters, and the inferred *m/n* value from the χ-disorder method is low (0.39) and from slope-area methods is high (0.7). Interestingly, our methodology, which can account for spatial gradients, infers an *m/n* value in between these two values (0.51). Further evidence of the effects of spatial gradients in previous studies can be found in the measured concavity index or *m/n* values of Himalayan rivers, measured as high using slope-area methods (Kirby & Whipple, 2001), and low with χ based methods (Gailleton et al., 2021).

4.2. Different Approaches to Counter the Influence of Spatial Gradients on River Networks

Spatial gradients in channel steepness index are created by spatial gradients in rock uplift or any factor that influences erodibility, such as precipitation. The impact of spatial gradients in normalized channel steepness is well understood (Goren et al., 2014; Han et al., 2015; Kirby & Whipple, 2001; Leonard & Whipple, 2021; Roe et al., 2002). Here, however, we assess the magnitude of this impact and how spatial gradients control the estimated value of *m/n* when using the presently widely adopted methodologies that is, the χ-based methods available in LSDTopoTools and TopoToolbox (Hergarten et al., 2016; Mudd, Clubb, Gailleton, & Hurst, 2018; Mudd, Clubb, Gailleton, Hurst, Milodowski, & Valters, 2018; Schwanghart & Scherler, 2014).

To prevent spatial variation in rock uplift and erodibility from influencing estimates of the concavity index, it can be useful to only measure concavity on rivers or portions of rivers in which the assumptions of steady-state and spatially uniform rock uplift and erodibility appear to be true (Kirby & Whipple, 2001; Snyder et al., 2000). Although this may constrain values of the concavity index and thus *m/n* more accurately, it requires ignoring the majority of the information contained in the river networks. It is arguably better to use an approach that uses as much data contained in the river networks as possible to ensure that the inferred *m/n* value is representative of the entire area. Furthermore, even though care is taken to ensure that there is no variation in any geological, tectonic and climate factors, it is unlikely that we can ever truly remove variation of these in real examples on earth.

Another approach to mitigate the influence of spatial gradients has been to incorporate precipitation data into the channel steepness index calculation (Adams et al., 2020; Leonard & Whipple, 2021). Orographic effects often create an increasing gradient in precipitation rates toward the headwaters of rivers, which influences the concavity index (Han et al., 2015; Roe et al., 2002). To prevent these changes in the concavity index reflecting changes in

the channel steepness index, some studies have weighted the channel steepness index with a precipitation or discharge parameter (Adams et al., 2020; Leonard & Whipple, 2021). Whilst this approach benefits from being able to isolate variation in precipitation from other variables, there are a few issues. First, the approach still relies on the assumption of spatially uniform rock uplift and erodibility although the influence of precipitation on erodibility is controlled. Second, by introducing modern-day precipitation rate data, a number of new assumptions are introduced. There is an assumption that either the landscape is in steady state with the modern-day precipitation rate, or the modern-day precipitation rate data is representative of the average precipitation rate experienced by the landscape over the timescale in which it achieves steady state. Furthermore, it is assumed that across the landscape, all precipitation is converted to runoff (Leonard & Whipple, 2021). Therefore, although the assumption of spatially invariant precipitation rates is removed, it is replaced by a number of other assumptions, and still relies on concavity index or m/n calculations from previous work. In contrast, the approach presented here directly images channel steepness variations and the resulting maps could be compared to maps of precipitation or rock uplift rate to assess how these parameters influence channel steepness index values. If, however, precipitation can be accurately constrained, it is straightforward to incorporate this into the calculation of χ and proceed with the method presented here to estimate the optimal value of m/n, and image other unknown spatial variations. In this respect, any known variability in precipitation rates or any other parameter could be incorporated into the calculation of χ or indeed any known controls on variability, such as faults or lithological contacts, can be directly incorporated into the discretization scheme.

4.3. The Impact of the m/n on Inferring Tectonics in the Clearwater Catchment

From thermochronometry, we know that the exhumation and rock uplift rates in the Clearwater catchment are approximately 3 times higher in the headwaters compared to the baselevel (Brandon et al., 1998; Michel et al., 2018). Given that the catchment is in steady state, and if we make the $n = 1$ assumption that has been justified in other locations in the western US (Schwanghart & Scherler, 2020; Smith et al., 2024), channel steepness index values should represent the normalized rock uplift rate (Kirby & Whipple, 2012; Smith et al., 2022). As lithology and precipitation rate are relatively invariant within the catchment (Prism Climate Group, 2014; Tabor & Cady, 1978), we may make the assumption that erodibility in the catchment is spatially invariant. Under these conditions, we would expect the channel steepness index values to scale linearly to the measured rock uplift rates.

Under these assumptions, the map of channel steepness index created with the correct value of concavity index should show values of channel steepness index tripling from the baselevel to the headwaters. The channel steepness index map in which this is the case is the map created with an m/n of 0.51 inferred using our inverse scheme. At different values of m/n, the inferred channel steepness index maps have different gradients to what is expected, and also have different spatial patterns. This latter point has been demonstrated previously (Gailleton et al., 2021), but we reemphasize it here to show how influential spatial gradients can be, not only for estimating m/n but also for interpretations beyond that.

4.4. m/n Estimates and Channel Steepness Index Map Reconciles Observations in the Mohand Range

The map of normalized channel steepness index for the Mohand Range, created using our best fit m/n value of 0.31 (Figure 10), reveals several gradients in channel steepness index across the range that can explain observations from previous studies. First, we select a band of high channel steepness index on the southwestern flank of the range. These high values correlate to the location of the stronger Lower/Middle Siwaliks, which corresponds to greater channel steepness index values (Kirby & Whipple, 2012; Wahyudi et al., 2021). For rivers draining the southwestern flank, the location of this lithological boundary causes the gradient in channel steepness index to increase from the headwaters to the lower reaches, leading to higher inferred values of m/n when using a χ-based method (Wahyudi et al., 2021). Interestingly, Kirby and Whipple (2012) also found high values for the concavity index when using a slope-area methodology, contrary to the predictions in Section 4.1. Kirby and Whipple (2012) separated their chosen river at the knickpoint caused by the lithological contact, and inferred a concavity index of 0.46 ± 0.15 for the upstream section, and a value of 0.73 ± 0.19 for the downstream section. This can be explained by examining the gradients on the normalized channel steepness index map (Figure 10).

The river networks draining the southwestern flank of the range can be split into two sections, where in the downstream portions, channel steepness index values are higher than in the upstream portions. This creates the

effect of decreasing values of channel steepness index within the catchment. However, within the two portions of the network, both above and below the lithological contact, the values of channel steepness index increase upstream. Measuring these portions of these river networks separately with a slope-area method causes concavity indices to be higher (Kirby & Whipple, 2012). We would thus expect the χ-based approach to measure lower values of *m/n*. However, because the χ-based approach does not split the network into two at the lithological contact, the large scale gradient this method samples is one of decreasing channel steepness index values in the upstream direction. This causes measured *m/n* values from the χ-based approach to also be higher (Wahyudi et al., 2021). As such, the two methods that typically estimate opposite trends in the concavity index or *m/n* for a given spatial gradient, produce similar values for the concavity index or *m/n*.

As we create a normalized channel steepness map for the entire range, we are also able to infer processes beyond that of a lithological control on the channel steepness index (Allen et al., 2013; Kirby & Whipple, 2012; Wahyudi et al., 2021). We observe higher values of channel steepness index in the center of the range that decrease to both the southwest and the northeast, and we also infer decreasing values of channel steepness index to the southwest within the higher channel steepness index values caused by the changing lithology. These gradients are imposed over the variation in channel steepness index values caused by lithology, and we may reasonably suggest that there is some other process creating gradients in the channel steepness index. Precipitation is relatively homogenous across the range (Shrestha et al., 2012), and we wouldn't expect noise, which should be stochastically distributed throughout the data set, to create the systematic gradients that are observed. As such, it is likely that variation in the channel steepness index is caused by rock uplift rate variation. On a cross-section from southwest to northeast across the range, we would observe two peaks in the channel steepness index: one at the lithological contact and one at the drainage divide. Values of channel steepness index decrease from these peaks to the southwest, and so it is possible that there is a gradient of decreasing channel steepness from the center of the range to the range front. However, the gradient in the high channel steepness index values from the southwestern portion of the rivers draining the southwestern flank is much greater than the gradient that acts on the upstream portions of those rivers. Thus, we might reasonably suggest that there are two gradients acting on these rivers that are independent of each other and are caused by two regions of high rock uplift across the range. In different locations in the Siwalik Hills, a double peak in rock uplift rate has been recovered, and is implicated with fault-bend folding (Lavé & Avouac, 2000), whereas a single peak in rock uplift is associated with fault-propagation folding (Srivastava et al., 2018). Our observations therefore support the hypothesis that the Mohand Range is being uplifted by a fault-bend fold.

5. Conclusions

Present methodologies to estimate *m/n* rely on an assumption of spatially invariant u^* values that rarely exist in nature. We have demonstrated that spatial gradients in the channel steepness index can result in systematic variation in the concavity index values of river networks, and the estimates of *m/n*. This causes issues when creating and interpreting maps of channel steepness index, an important and useful tool in tectonic geomorphology, because the tools developed to estimate *m/n* assume uniform channel steepness values. We provide an alternative means of constraining *m/n* based on a topographic inversion that does not require a spatially invariant channel steepness index. We have shown that our methodology is able to accurately constrain the *m/n* value used to create a synthetic landscape, without requiring different catchments to have different *m/n* values. In the case of the Clearwater catchment, we recover a value of *m/n* that can be used to correctly recover the gradient in rock uplift inferred from other data sets. Having shown that other methods to estimate the concavity index or *m/n* are impacted by the spatial gradient in rock uplift in the Clearwater catchment, we apply our methodology to the Mohand Range in the Siwalik Hills, where gradients in rock uplift are less well constrained. We constrain an *m/n* of 0.31 for the Mohand Range, lower than previous estimates for the Siwalik Hills (Kirby & Whipple, 2001). We use this value of *m/n* to create a map of channel steepness index, allowing us to reconcile observations of rock uplift rate and lithological change and explain why reported values of concavity and *m/n* have been variable (Kirby & Whipple, 2012; Wahyudi et al., 2021). Our new methodology to estimate *m/n* represents a powerful tool for investigating tectonic and climatic changes in landscapes and highlights the utility of inverse methods in tectonic geomorphology.

Data Availability Statement

The code required to calculate *m/n* using our inverse method is available from this zenodo repository (Smith, 2024), which can be found on Github at https://github.com/adamsmith142/INCA.

Acknowledgments
AS would like to acknowledge Andrew Carter for his continued support and supervision and Mark Brandon for stimulating discussions that inspired this research. We also wish to thank Aaron Bufe, Stefan Hergarten, the Associate Editor and an anonymous reviewer for comments that greatly improved this manuscript. AS is supported by the Natural Environment Research Council (NE/S007229/1).

References

Adams, B. A., Whipple, K. X., Forte, A. M., Heimsath, A. M., & Hodges, K. V. (2020). Climate controls on erosion in tectonically active landscapes. *Science Advances*, *6*(42), eaaz3166. https://doi.org/10.1126/sciadv.aaz3166

Allen, G. H., Barnes, J. B., Pavelsky, T. M., & Kirby, E. (2013). Lithologic and tectonic controls on bedrock channel form at the northwest Himalayan front. *Journal of Geophysical Research: Earth Surface*, *118*(3), 1806–1825. https://doi.org/10.1002/jgrf.20113

Anders, M. H., Spiegelman, M., Rodgers, D. W., & Hagstrum, J. T. (1993). The growth of fault-bounded tilt blocks. *Tectonics*, *12*(6), 1451–1459. https://doi.org/10.1029/93TC01547

Armstrong, P. A., Ehlers, T. A., Chapman, D. S., Farley, K. A., & Kamp, P. J. J. (2003). Exhumation of the central Wasatch Mountains, Utah: 1. Patterns and timing of exhumation deduced from low-temperature thermochronology data. *Journal of Geophysical Research*, *108*(B3), 2172. https://doi.org/10.1029/2001JB001708

Avouac, J.-P. (2003). Mountain building, erosion, and the seismic cycle in the Nepal Himalaya: Amsterdam, Elsevier. *Advances in Geophysics*, *46*, 1–80.

Barnes, J. B., Densmore, A. L., Mukul, M., Sinha, R., Jain, V., & Tandon, S. K. (2011). Interplay between faulting and base level in the development of Himalayan frontal fold topography. *Journal of Geophysical Research*, *116*(F3), F03012. https://doi.org/10.1029/2010JF001841

Brandon, M. T., Roden-Tice, M. K., & Garver, J. I. (1998). Late Cenozoic exhumation of the Cascadia accretionary wedge in the Olympic Mountains, northwest Washington State. *Geological Society of America Bulletin*, *110*(8), 985–1009. https://doi.org/10.1130/0016-7606(1998)110<0985:LCEOTC>2.3.CO;2

Braun, J., & Willett, S. D. (2013). A very efficient O(*n*), implicit and parallel method to solve the stream power equation governing fluvial incision and landscape evolution. *Geomorphology*, *180–181*, 170–179. https://doi.org/10.1016/j.geomorph.2012.10.008

Buck, W. R. (1988). Flexural rotation of normal faults. *Tectonics*, *7*(5), 959–973. https://doi.org/10.1029/TC007i005p00959

Bufe, A., Paola, C., & Burbank, D. W. (2016). Fluvial bevelling of topography controlled by lateral channel mobility and uplift rate. *Nature Geoscience*, *9*, 706–710. https://doi.org/10.1038/ngeo2773

Burbank, D. W., Leland, J., Fielding, E., Anderson, R. S., Brozovic, N., Reid, M. R., & Duncan, C. (1996). Bedrock incision, rock uplift and threshold hillslopes in the northwestern Himalayas. *Nature*, *379*(6565), 505–510. https://doi.org/10.1038/379505a0

Burgess, W., Yin, A., Dubey, C. S., Shen, Z.-K., & Kelty, T. K. (2012). Holocene shortening across the Main Frontal Thrust zone in the eastern Himalaya. *Earth and Planetary Science Letters*, *357–358*, 152–167. https://doi.org/10.1016/j.epsl.2012.09.040

Farr, T. G., Rosen, P. A., Caro, E., Crippen, R., Duren, R., Hensley, S., et al. (2007). The Shuttle Radar Topography Mission. *Reviews of Geophysics*, *45*(2), RG2004. https://doi.org/10.1029/2005RG000183

Flint, J. J. (1974). Stream gradient as a function of order, magnitude, and discharge. *Water Resources Research*, *10*(5), 969–973. https://doi.org/10.1029/WR010i005p00969

Fox, M., Clinger, A., Smith, A. G. G., Cuffey, K., Shuster, D., & Herman, F. (2024). Antarctic Peninsula glaciation patterns set by landscape evolution and dynamic topography. *Nature Geoscience*, *17*(1), 73–78. https://doi.org/10.1038/s41561-023-01336-7

Gailleton, B., Mudd, S. M., Clubb, F. J., Grieve, S. W. D., & Hurst, M. D. (2021). Impact of changing concavity indices on channel steepness and divide migration metrics. *Journal of Geophysical Research: Earth Surface*, *126*(10), e2020JF006060. https://doi.org/10.1029/2020JF006060

Gansser, A. (1964). *Geology of the Himalayas*. Wiley.

Goren, L., Fox, M., & Willett, S. D. (2014). Tectonics from fluvial topography using formal linear inversion: Theory and applications to the Inyo Mountains, California. *Journal of Geophysical Research: Earth Surface*, *119*(8), 1651–1681. https://doi.org/10.1002/2014JF003079

Hack, J. T. (1957). Studies of longitudinal stream profiles in Virginia and Maryland, *USGS Shorter Contributions to General Geology Geological Survey Professional Paper 294-B* (pp. 45–95).

Han, J., Gasparini, N. M., & Johnson, J. P. L. (2015). Measuring the imprint of orographic rainfall gradients on the morphology of steady-state numerical fluvial landscapes. *Earth Surface Processes and Landforms*, *40*(10), 1334–1350. https://doi.org/10.1002/esp.3723

Hansen, P. C. (1992). Analysis of discrete ill-posed problems by means of the L-curve. *SIAM Review*, *34*(4), 561–580. https://doi.org/10.1137/1034115

Harkins, N., Kirby, E., Heimsath, A., Robinson, R., & Reiser, U. (2007). Transient fluvial incision in the headwaters of the Yellow River, northeastern Tibet, China. *Journal of Geophysical Research*, *112*(F3), F03S04. https://doi.org/10.1029/2006JF000570

Hergarten, S., Robl, J., & Stüwe, K. (2016). Tectonic geomorphology at small catchment sizes – Extensions of the stream-power approach and the χ method. *Earth Surface Dynamics*, *4*, 1–9. https://doi.org/10.5194/esurf-4-1-2016

Howard, A. D. (1994). A detachment-limited model of drainage basin evolution. *Water Resources Research*, *30*(7), 2261–2285. https://doi.org/10.1029/94WR00757

Howard, A. D., & Kerby, G. (1983). Channel changes in badlands. *GSA Bulletin*, *94*(6), 739–752. https://doi.org/10.1130/0016-7606(1983)94<739:CCIB>2.0.CO;2

Hurtrez, J.-E., Lucazeau, F., Lavé, J., & Avouac, J.-P. (1999). Investigation of the relationships between basin morphology, tectonic uplift, and denudation from the study of an active fold belt in the Siwalik Hills, central Nepal. *Journal of Geophysical Research*, *104*(B6), 12779–12796. https://doi.org/10.1029/1998JB900098

Kirby, E., & Whipple, K. (2001). Quantifying differential rock-uplift rates via stream profile analysis. *Geology*, *29*(5), 415–418. https://doi.org/10.1130/0091-7613(2001)029<0415:QDRURV>2.0.CO;2

Kirby, E., & Whipple, K. X. (2012). Expression of active tectonics in erosional landscapes. *Journal of Structural Geology*, *44*, 54–75. https://doi.org/10.1016/j.jsg.2012.07.009

Lague, D. (2014). The stream power river incision model: Evidence, theory and beyond. *Earth Surface Processes and Landforms*, *39*(1), 38–61. https://doi.org/10.1002/esp.3462

Lavé, J., & Avouac, J. P. (2000). Active folding of fluvial terraces across the Siwaliks Hills, Himalayas of central Nepal. *Journal of Geophysical Research*, *105*(B3), 5735–5770. https://doi.org/10.1029/1999JB900292

Lavé, J., & Avouac, J. P. (2001). Fluvial incision and tectonic uplift across the Himalayas of central Nepal. *Journal of Geophysical Research*, *106*(B11), 26561–26591. https://doi.org/10.1029/2001JB000359

Leonard, J. S., & Whipple, K. X. (2021). Influence of spatial rainfall gradients on river longitudinal profiles and the topographic expression of spatially and temporally variable climates in mountain landscapes. *Journal of Geophysical Research: Earth Surface*, *126*(12), e2021JF006183. https://doi.org/10.1029/2021JF006183

Menke, W. (2012). *Geophysical data analysis: Discrete inverse theory* (p. 293). Academic Press.

Michel, L., Ehlers, T. A., Glotzbach, C., Adams, B. A., & Stübner, K. (2018). Tectonic and glacial contributions to focused exhumation in the Olympic Mountains, Washington, USA. *Geology*, *46*(6), 491–494. https://doi.org/10.1130/G39881.1

Morisawa, M. E. (1962). Quantitative geomorphology of some watersheds in the Appalachian Plateau. *Geological Society of America Bulletin*, *73*(9), 1025. https://doi.org/10.1130/0016-7606(1962)73[1025:QGOSWI]2.0.CO;2

Mudd, S. M., Attal, M., Milodowski, D. T., Grieve, S. W. D., & Valters, D. A. (2014). A statistical framework to quantify spatial variation in channel gradients using the integral method of channel profile analysis. *Journal of Geophysical Research: Earth Surface*, *119*(2), 138–152. https://doi.org/10.1002/2013JF002981

Mudd, S. M., Clubb, F. J., Gailleton, B., & Hurst, M. D. (2018). How concave are river channels? *Earth Surface Dynamics*, *6*(2), 505–523. https://doi.org/10.5194/esurf-6-505-2018

Mudd, S. M., Clubb, F. J., Gailleton, B., Hurst, M. D., Milodowski, D. T., & Valters, D. A. (2018). *The LSDTopoTools Chi Mapping Package*. Zenodo. https://doi.org/10.5281/ZENODO.1291889

Parker, R. L. (1994). *Geophysical inverse theory*. Princeton University Press. https://doi.org/10.1515/9780691206837

Pazzaglia, F. J., & Brandon, M. T. (2001). A fluvial record of long-term steady-state uplift and erosion across the Cascadia forearc high, western Washington State. *American Journal of Science*, *301*(4–5), 385–431. https://doi.org/10.2475/ajs.301.4-5.385

Perron, J. T., & Royden, L. (2013). An integral approach to bedrock river profile analysis. *Earth Surface Processes and Landforms*, *38*(6), 570–576. https://doi.org/10.1002/esp.3302

Powers, P. M., Lillie, R. J., & Yeats, R. S. (1998). Structure and shortening of the Kangra and Dehra Dun reentrants, sub-Himalaya, India. *Geological Society of America Bulletin*, *110*(8), 1010–1027. https://doi.org/10.1130/0016-7606(1998)110<1010:SASOTK>2.3.CO;2

Prism Climate Group. (2014). Retrieved from https://prism.oregonstate.edu

Raiverman, V., Mukerjea, A., Saproo, M. K., Kunte, S. V., & Ram, J. (1990). *Geological map of Himalayan foothills between Yamuna and Sarda rivers*. Institute of Petroleum Exploration.

Reiners, P. W., Ehlers, T. A., Mitchell, S. G., & Montgomery, D. R. (2003). Coupled spatial variations in precipitation and long-term erosion rates across the Washington Cascades. *Nature*, *426*(6967), 645–647. https://doi.org/10.1038/nature02111

Riebe, C. S., Sklar, L. S., Lukens, C. E., & Shuster, D. L. (2015). Climate and topography control the size and flux of sediment produced on steep mountain slopes. *Proceedings of the National Academy of Sciences*, *112*(51), 15574–15579. https://doi.org/10.1073/pnas.1503567112

Roberts, G. G., White, N. J., Martin-Brandis, G. L., & Crosby, A. G. (2012). An uplift history of the Colorado Plateau and its surroundings from inverse modeling of longitudinal river profiles. *Tectonics*, *31*(4), TC4022. https://doi.org/10.1029/2012TC003107

Roe, G. H., Montgomery, D. R., & Hallet, B. (2002). Effects of orographic precipitation variations on the concavity of steady-state river profiles. *Geology*, *30*(2), 143–146. https://doi.org/10.1130/0091-7613(2002)030<0143:EOOPVO>2.0.CO;2

Roe, G. H., Montgomery, D. R., & Hallet, B. (2003). Orographic precipitation and the relief of mountain ranges. *Journal of Geophysical Research*, *108*(B6), 2001JB001521. https://doi.org/10.1029/2001JB001521

Royden, L., Clark, M., & Whipple, K. (2000). Evolution of river elevation profiles by bedrock incision: Analytical solutions for transient river profiles related to changing uplift and precipitation rates. *Eos, Transactions American Geophysical Union*, *81*(48).

Schwanghart, W., & Scherler, D. (2014). Short Communication: TopoToolbox 2 – MATLAB-based software for topographic analysis and modeling in Earth surface sciences. *Earth Surface Dynamics*, *2*, 1–7. https://doi.org/10.5194/esurf-2-1-2014

Schwanghart, W., & Scherler, D. (2020). Divide mobility controls knickpoint migration on the Roan Plateau (Colorado, USA). *Geology*, *48*(7), 698–702. https://doi.org/10.1130/G47054.1

Shrestha, D., Singh, P., & Nakamura, K. (2012). Spatiotemporal variation of rainfall over the central Himalayan region revealed by TRMM Precipitation Radar. *Journal of Geophysical Research*, *117*(D22), 2012JD018140. https://doi.org/10.1029/2012JD018140

Smith, A. G. G. (2024). *adamsmith142/INCA: INCA 1.0*. Zenodo. https://doi.org/10.5281/ZENODO.11282900

Smith, A. G. G., Fox, M., Moore, J. R., Miller, S. R., Goren, L., Morriss, M. C., & Carter, A. (2024). One million years of climate-driven rock uplift rate variation on the Wasatch Fault revealed by fluvial topography. *American Journal of Science*, *324*. https://doi.org/10.2475/001c.92194

Smith, A. G. G., Fox, M., Schwanghart, W., & Carter, A. (2022). Comparing methods for calculating channel steepness index. *Earth-Science Reviews*, *227*, 103970. https://doi.org/10.1016/j.earscirev.2022.103970

Snyder, N. P., Whipple, K. X., Tucker, G. E., & Merritts, D. J. (2000). Landscape response to tectonic forcing: Digital elevation model analysis of stream profiles in the Mendocino triple junction region, northern California. *Geological Society of America Bulletin*, *112*(8), 1250–1263. https://doi.org/10.1130/0016-7606(2000)112<1250:lrttfd>2.0.co;2

Srivastava, V., Mukul, M., & Barnes, J. B. (2016). Main Frontal thrust deformation and topographic growth of the Mohand Range, northwest Himalaya. *Journal of Structural Geology*, *93*, 131–148. https://doi.org/10.1016/j.jsg.2016.10.009

Srivastava, V., Mukul, M., Barnes, J. B., & Mukul, M. (2018). Geometry and kinematics of Main Frontal thrust-related fault propagation folding in the Mohand Range, northwest Himalaya. *Journal of Structural Geology*, *115*, 1–18. https://doi.org/10.1016/j.jsg.2018.06.022

Tabor, R. W., & Cady, W. M. (1978). Geologic map of the Olympic Peninsula, Washington. *USGS Miscellaneous Investigations Series Map I-994*. https://doi.org/10.3133/i994

Tikhonov, A. N., & Arsenin, V. I. (1977). *Solutions of ill-posed problems*. *Scripta series in mathematics* (p. 258). Distributed Solely by Halsted Press.

Wahyudi, D. R., Sinclair, H. D., & Mudd, S. M. (2021). Progressive evolution of thrust fold topography in the frontal Himalaya. *Geomorphology*, *384*, 107717. https://doi.org/10.1016/j.geomorph.2021.107717

Wesnousky, S. G., Kumar, S., Mohindra, R., & Thakur, V. C. (1999). Uplift and convergence along the Himalayan Frontal Thrust of India. *Tectonics*, *18*(6), 967–976. https://doi.org/10.1029/1999TC900026

Whipple, K. X., & Tucker, G. E. (1999). Dynamics of the stream-power river incision model: Implications for height limits of mountain ranges, landscape response timescales, and research needs. *Journal of Geophysical Research*, *104*(B8), 17661–17674. https://doi.org/10.1029/1999JB900120

Whittaker, A. C. (2012). How do landscapes record tectonics and climate? *Lithosphere*, *4*(2), 160–164. https://doi.org/10.1130/RF.L003.1

Willett, S. D. (1999). Orogeny and orography: The effects of erosion on the structure of mountain belts. *Journal of Geophysical Research*, *104*(B12), 28957–28981. https://doi.org/10.1029/1999JB900248

Willett, S. D., McCoy, S. W., Perron, J. T., Goren, L., & Chen, C.-Y. (2014). Dynamic reorganization of river basins. *Science*, *343*(6175), 1248765. https://doi.org/10.1126/science.1248765

Wobus, C., Whipple, K. X., Kirby, E., Snyder, N., Johnson, J., Spyropolou, K., et al. (2006). Tectonics from topography: Procedures, promise, and pitfalls. *Special Papers - Geological Society of America*, *398*, 55.

Yeats, R. S., & Lillie, R. J. (1991). Contemporary tectonics of the Himalayan frontal fault system: Folds, blind thrusts and the 1905 Kangra earthquake. *Journal of Structural Geology*, *13*(2), 215–225. https://doi.org/10.1016/0191-8141(91)90068-T

Yeats, R. S., & Thakur, V. C. (2008). Active faulting south of the Himalayan Front: Establishing a new plate boundary. *Tectonophysics*, *453*(1–4), 63–73. https://doi.org/10.1016/j.tecto.2007.06.017

Yin, A. (2006). Cenozoic tectonic evolution of the Himalayan orogen as constrained by along-strike variation of structural geometry, exhumation history, and foreland sedimentation. *Earth-Science Reviews*, *76*(1–2), 1–131. https://doi.org/10.1016/j.earscirev.2005.05.004